

Carboplatin- and Etoposide-Loaded Lactoferrin Protein Nanoparticles for Targeting Cancer Stem Cells in Retinoblastoma In Vitro

Revu V. L. Narayana,¹ Pritikana Jana,² Neha Tomar,² Varsha Prabhu,¹ Rohini M. Nair,^{1,3} Radhika Manukonda,¹ Swathi Kaliki,^{4,5} Sarah E. Coupland,^{6,7} Jodi Alexander,^{6,8} Helen Kalirai,^{6,7} Anand K. Kondapi,² and Geeta K. Vemuganti¹

¹School of Medical Sciences, University of Hyderabad, Hyderabad, India

²Department of Biotechnology and Bioinformatics, School of Life Sciences, University of Hyderabad, Hyderabad, India

³Department of Ophthalmology, Perelman School of Medicine, University of Pennsylvania, Philadelphia, United States

⁴The Operation Eyesight Universal Institute for Eye Cancer, L V Prasad Eye Institute, Hyderabad, India

⁵Ophthalmic Pathology Laboratory, L V Prasad Eye Institute, Hyderabad, India

⁶Liverpool Ocular Oncology Research Group, Department of Molecular and Clinical Cancer Medicine, Institute of Systems, Molecular and Integrative Biology (ISMIB), University of Liverpool, Liverpool, United Kingdom

⁷Liverpool Clinical Laboratories, Liverpool University Hospitals Foundation Trust, Liverpool, United Kingdom

⁸School of Biological Sciences, Brambell Laboratories, Bangor University, Bangor, United Kingdom

Correspondence: Geeta K. Vemuganti, School of Medical Sciences, University of Hyderabad, Hyderabad-500046, India; gkvemuganti@gmail.com, gvmd.uoh@nic.in.

Received: December 7, 2020

Accepted: August 12, 2021

Published: November 16, 2021

Citation: Narayana RVL, Jana P, Tomar N, et al. Carboplatin- and etoposide-loaded lactoferrin protein nanoparticles for targeting cancer stem cells in retinoblastoma in vitro. *Invest Ophthalmol Vis Sci.* 2021;62(14):13. <https://doi.org/10.1167/iovs.62.14.13>

PURPOSE. Cancer stem cells (CSCs) are known to contribute to tumor relapses by virtue of their chemoresistance. With the knowledge that nanoformulations can overcome drug resistance, we evaluated the efficacy and cytotoxicity of clinical-grade carboplatin (CPT)- and etoposide (ETP)-loaded lactoferrin nanoparticles (Lf-Nps) on total, CD133-enriched (non-CSC), and CD133-depleted (CSC) populations of retinoblastoma (Rb) Y79 cells.

METHODS. Physicochemical properties of drug-loaded Lf-Nps were measured with transmission electron microscopy and attenuated total reflectance-Fourier transform infrared. The encapsulation efficiency, uptake, and release of drug-loaded Lf-Nps were measured using high-performance liquid chromatography and a UV-visible spectrophotometer. Cytotoxicity of the standard and drug-loaded Lf-Nps was evaluated by the MTT assay.

RESULTS. The mean (SD) size and encapsulation efficiency of Lf-CPT and Lf-ETP were 61.2 (3.94) nm, 60% and 45.15 (5.85) nm, 38%, respectively, and the drug release efficiency was highest at pH 6. The increased drug uptake and lower release of drug-loaded Lf-Nps were observed in CSC and non-CSC populations compared to their standard forms. The relative increase of drug uptake and sustained intracellular retention of the drug-loaded Lf-Nps compared to standard drugs showed an enhanced cytotoxicity up to 50%, especially in Rb Y79 CSCs (IC₅₀: CPT, 230.3; Lf-CPT, 118.2; ETP, 198.1; and Lf-ETP, 129) compared to non-CSCs.

CONCLUSIONS. Our study documents an increase in drug uptake, retention, and cytotoxicity of Lf-CPT and Lf-ETP on Y79 CSCs and non-CSCs as compared to their standard drugs in vitro. The reversal of chemoresistance in the CSC population by nanoformulation appears promising with the potential to pave the way for improved targeted therapy and better clinical outcomes.

Keywords: retinoblastoma, cancer stem cells, carboplatin, etoposide, lactoferrin nanoparticles

Retinoblastoma (Rb) is the most common pediatric intraocular malignancy, with an incidence ranging from 1 in 16,000 to 1 in 18,000 live births and representing 4% of all pediatric tumors.¹ Due to advanced diseases at presentation in some low- and middle-income countries, Rb cases can show high clinical and histologic risk factors (e.g., invasion into the optic nerve, choroid, sclera, and the anterior chamber of the eye) and may also metastasize to the central nervous system (CNS) and bone marrow, as confirmed by evaluation of cerebrospinal fluid and bone marrow cytologic

examination.^{2,3} Multimodal treatment options are required because of the low survival rate associated with metastatic Rb. The current treatment options include enucleation, radiotherapy, cryotherapy, thermotherapy, and chemotherapy, depending on tumor size, location, and stage.⁴ In view of the advanced disease at presentation in India, neoadjuvant (before enucleation) or systemic adjuvant (after enucleation) chemotherapy is one of the most common treatment modalities for treating Rb. Different combinations of standard therapeutic agents, such as carboplatin (CPT, a

DNA alkylating agent) and etoposide (ETP, a topoisomerase inhibitor), are commonly administered for treating Rb with minimal side effects.^{5,6} Successful treatment of Rb occurs in ~90% of patients, especially in developed countries; however, Rb remains a potentially life-threatening pediatric disease because of recurrence or relapse.^{7,8} Our observation, presented at the International Congress of Ocular Oncology (ICOO) 2009, of tumor cell persistence, including undifferentiated cells in the enucleated eyes of children with advanced Rb after chemotherapy,⁹ stimulated us to examine further the efficacy and sensitivity of the tumor cells to drugs. As seen in other tumors, we speculated that the viable Rb cells in the enucleated specimens could possibly be due to chemoresistant properties of cancer stem cells (CSCs) residing in the tumor.^{10,11} In agreement with the evidence in other solid cancers,¹² several studies have documented the presence of CSCs in primary Rb as well as in Rb cell lines, such as Rb Y79 and WERI-Rb cells.^{13,14} Our group also reported the CSC population in both primary Rb and Y79 cells, which were identified as a CD133^{lo} population,^{15,16} and we also demonstrated that these CSCs were resistant to CPT in *in vitro* cytotoxicity assays.¹⁶

CSCs are small population of cells within a tumor that exhibit stem cell-like properties, such as self-renewal and differentiation to heterogeneous lineage, and also cause tumorigenesis and metastasis.¹⁷ CSCs can induce cell cycle arrest, leading to a quiescent state and the ability to become resistant to chemotherapeutic drugs, most of which target proliferating cells during the cell cycle. Since the CSCs are known to be in a quiescent state, they are assumed to be one of the mechanisms leading to evasion of cytotoxicity and contributing to therapeutic resistance.^{18,19} Nanoparticle-mediated drug delivery has emerged as a promising tool to overcome drug resistance mechanisms in CSCs. Nanomaterials developed to target CSCs in *in vivo* and *in vitro* studies include carbon, metal, polymer, and liposomal-based nanomaterials, loaded with inhibitory molecules, small interfering RNA/microRNA, and therapeutic cancer drugs.²⁰ Protein nanoparticles have been explored as they are nontoxic, biodegradable, and easily metabolized, and they possess good biocompatibility. Moreover, the amphiphilic nature of proteins helps them to interact with both hydrophilic and hydrophobic drugs. The abundance of charged groups in proteins makes them susceptible to chemical modifications and to covalent or noncovalent interactions with drugs. This property offers an excellent opportunity for surface modifications of proteins, and the drugs can be physically entrapped with the proteins.²¹ In order to improve target specificity, lactoferrin (Lf) protein serves for target recognition as well as the drug carrier for localization in target cells.

Various nanoparticles and drugs have been investigated for efficacy against Rb^{22,23}; however, their effectiveness in targeting the CSC populations within the tumor has not been addressed. In this study, we evaluated the efficacy and cytotoxicity of CPT and ETP, used in clinical practice, and compared them with the nanoformulations of the same drugs using the Rb Y79 cell line, specifically the cells endowed with CSC properties (i.e., CD133^{lo}).

MATERIALS AND METHODS

Materials

Lf protein was purchased from Vitacost (Florida, USA). Pure forms of CPT, ETP, and rhodamine 6G (R6G) fluorescent dyes were purchased from Sigma-Aldrich (St. Louis, MO, USA).

Clinical-grade drugs of CPT and ETP were purchased from Alkem Laboratories Ltd. (Mumbai, India) and Cadila Healthcare Ltd. (Ahmedabad, India), respectively. CD133 magnetic-activated cell sorting (MACS) microbeads were purchased from Miltenyi Biotech (Bergisch Gladbach, Germany). 3-(4,5-Dimethylthiazol-2-yl)-2,5-diphenyltetrazolium bromide (MTT) was purchased from Thermo Fisher Scientific (MA, USA). All analytical grade reagents and solvents were purchased from Sigma-Aldrich.

Preparation of CPT-, ETP-, and R6G-Loaded Lactoferrin Nanoparticles

Lf-CPT, Lf-ETP, and Lf-R6G were prepared as per the previously described solution-oil chemistry method.²⁴ Briefly, the drug and Lf (dissolved in 1× PBS, pH 7.4) were mixed at the ratio of 1:4 and incubated on ice for 60 minutes. This mixture was slowly added to 25 mL of olive oil (Leonardo, Italy) while stirring and incubated on ice for 30 minutes. The samples were sonicated using a narrow stepped titanium probe of ultrasonic homogenizer (300V/T; Biologics, Inc., Manassas, VA, USA) for 15 minutes at 4°C. After this, samples were frozen in liquid N₂ for 10 minutes and immediately transferred to 4°C and incubated for 4 hours. The mixture was pelleted by centrifugation at 6000 rpm for 10 minutes, and the pellet was washed three times with diethyl ether and resuspended in 1× PBS (pH 7.4).

Physicochemical Characterization of Drug-Loaded Lactoferrin Nanoparticles

Transmission Electron Microscopy Analysis. Lf-CPT, Lf-ETP, and lactoferrin nanoparticles (Lf-Nps) were fixed on a 200-mesh type B carbon-coated copper grid and stained with 2% uranyl acetate and captured with FEI TECNAI G2S-TWIN 200-kV electron microscope (FEI, Germany).

Attenuated Total Reflected-Fourier Transform Infrared Analysis. Attenuated total reflected-Fourier transform infrared (ATR-FTIR) analysis was performed by ATR (Bruker, Bremen, Germany), managed by Bruker OPUS 7.0 software. A drop of lyophilized CPT, ETP, Lf-CPT, Lf-ETP, and Lf-Nps was placed on the diamond probe followed by scanning in a range of 500 to 4000 cm⁻¹ wavelength, and analysis of spectra was performed using essential FTIR software.

HPLC Analysis for Drug Encapsulation Efficiency and Loading Capacity. Encapsulation efficiency and loading capacity of the drugs in Lf-Nps were determined using reverse-phase HPLC (Waters 2695; Waters, MA, USA) with a UV detector (Waters 2487). Lf-CPT, Lf-ETP, and Lf-Nps were dissolved in 500 μL PBS at pH 5.5 for drug release and placed on a rocker at room temperature for 4 hours. To precipitate the protein, 50 μg proteinase K (dissolved in double-distilled water) was added to Lf-CPT, and 50 μL 30% AgNO₃ was added to Lf-ETP. Released drugs were extracted by adding 450 μL HPLC-grade MilliQ and methanol for CPT and ETP, respectively. The mixture was centrifuged at 12,000 rpm for 15 minutes, and the supernatant was filtered with a 0.2-μm syringe filter and collected into HPLC vials. Released drugs were quantified using HPLC. The analytical column used was a reverse-phase C18 column. The mobile phase of CPT was 100% MilliQ water with a 1-mL/min flow rate and mixture of acetonitrile and MilliQ water (40:60) for ETP. The column

effluent was detected by their absorption at 220 nm for CPT and at 284 nm for ETP. Quantification was performed from the standard curve of known drug concentrations. The encapsulation efficiency was calculated using the following equations:

$$\text{Encapsulation efficiency (\%)} = \frac{\text{Actual amount of drug loaded in nanoparticle}}{\text{Initial amount of drug}} * 100$$

$$\text{Loading capacity (\%)} = \frac{\text{Amount of drug entrapped}}{\text{Weight of nanoparticle}} * 100$$

pH-Dependent Drug Release. Equivalent 200 µg Lf-CPT and Lf-ETP were suspended in 1 mL PBS of different pH ranges (1–10). The mixture was incubated with gentle shaking at 200 rpm for 4 hours. The samples were collected at different time intervals and centrifuged at 15,000 rpm for 15 minutes. The absorbance of CPT and ETP was measured by a spectrophotometer at 220 nm and 280 nm. The concentration of CPT and ETP was calculated using a standard curve of known concentrations to estimate the drug release from the Lf-CPT and Lf-ETP at different pH ranges.

Cell Culture and Isolation of Cancer Stem Cells

Rb Y79 cell line was obtained from Riken (Japan) (RCB-1645), and the cells were grown in RPMI-1640 (Gibco, Thermo Fisher Scientific) medium supplemented with 10% fetal bovine serum (Gibco, Thermo Fisher Scientific) along with 1× antibiotic-antimycotic (Gibco, Thermo Fisher Scientific) at 5% CO₂ and 37°C. The medium was changed every 48 hours and cells subcultured until they reached 80% confluency. Cell number and viability were routinely assessed by trypan blue dye exclusion method using a Neubauer chamber.

The subcultured Rb Y79 cells were sorted using CD133 antibody as previously described.¹⁶ Briefly, Rb Y79 cells were washed with 2 mM EDTA MACS buffer (pH 7.2) and resuspended in 300 µL MACS buffer. Cells were blocked with 100 µL F_{cR} blocking reagent (Miltenyi Biotech) and incubated with 100 µL CD133 microbeads (Miltenyi Biotech) at 4°C for 30 minutes. The cell mixture was passed through an activated LS mini-MACS column (Miltenyi Biotech) followed by repeated washing with a MACS buffer. The unbound CD133^{lo} cells were eluted first and collected in a tube with media. The column was then removed from the magnet, and CD133^{hi} fractions were collected by flushing with nozzle. Both viability and cell number in CD133^{lo/hi} populations were assessed by a Neubauer chamber, and the purity of sorted cells was analyzed by flow cytometry (BD LSR Fortessa, CA, USA).

Cellular Uptake of Lf-Nps by Confocal Microscopy. Rb Y79 cells were seeded at a density of 5 × 10⁵ per 35-mm cell culture dish with 3 mL serum-free RPMI-1640 containing the equivalent concentration of 20 µg R6G or Lf-R6G. Cells were harvested at different time intervals (30, 60, 120, 240, and 480 minutes), washed with 1× PBS, and mounted on a glass slide with 50% glycerol. The intracellular concentration of dye and nanoparticles was assessed using laser confocal microscopy (Carl Zeiss, Jena, Germany) at 450/550-nm emission absorption fluorescence spectra.

Cellular Uptake Assay by Quantitative Measurement of Drugs and Nanoparticles. Rb Y79 cells were seeded at a density of 1 × 10⁶ in 3-mL serum-free RPMI-1640 medium in a 35-mm cell culture dish and incubated

for 1 hour. Equivalent concentrations of 100 µg CPT, ETP, Lf-CP, and Lf-ETP each were added to the culture dishes. After incubation, cells were washed with 1× PBS (pH 7.4) and lysed with 1 mL 1% Triton-100 at different time intervals (30 minutes, 1 hour, 2 hours, 4 hours, 8 hours, 16 hours, 24 hours, 36 hours, and 48 hours). The cell lysate was discarded by centrifugation at 1200 rpm at 4°C for 20 minutes. The supernatant was collected and the protein was precipitated by adding an equal volume of acetonitrile to the supernatant and incubated overnight at 4°C. The mixture was centrifuged at 12,000 rpm for 15 minutes, the supernatant was collected, and the concentrations of CPT and ETP were quantified by a UV-Vis spectrophotometer at 220 nm and 280 nm, respectively.

Quantitative Measurement of Drug Uptake by Rb Y79 CSCs and Non-CSCs. Rb Y79 CSCs and non-CSCs were seeded at a density of 1 × 10⁶ cells in 3 mL serum-free RPMI-1640 medium for 1 hour in a 35-mm cell culture dish. Cells were treated with 100-µg equivalent concentrations of CPT, ETP, Lf-CPT, and Lf-ETP and incubated for 4 hours. After incubation, cells were washed with 1× PBS (pH 7.4), and drug uptake was measured by a UV-Vis spectrophotometer described in above method.

Estimation of Drug Available in Conditioned Media of Rb Y79 CSCs and Non-CSCs. Quantitative estimation of free drug available in conditioned media of CPT-, ETP-, Lf-CPT-, and Lf-ETP-treated Rb Y79 total, CSCs, and non-CSCs was performed using a UV-Vis spectrophotometer. The sorted Rb Y79 cells were seeded at a density of 1 × 10⁶ cells in 3 mL serum-free RPMI-1640 medium for 1 hour in a 35-mm cell culture dish. Around 100-µg equivalent concentrations of CPT, ETP, Lf-CPT, and Lf-ETP were added to the culture dishes and incubated for 4 hours. After incubation, cells were washed with 1× PBS (pH 7.4) and resuspended in 1 mL serum-free RPMI-1640 medium. At different time points, conditioned media were collected and estimated free drug against the standard curve normalized with serum-free RPMI-1640. The percentage of drug retention into the cells was calculated using the following formula:

$$\text{Drug Retention (\%)} = \frac{(\text{Mean of drug uptake by 48 hours}) - (\text{Mean of drug available in conditional media after 48 hours})}{\text{Mean of drug uptake by 48 hours}} * 100$$

Cytotoxic Effect of Standard Drugs and Nanoparticles in Y79 Rb Total, CSCs, and Non-CSCs. The cytotoxic effect of standard drugs, Lf-Nps, and drug-loaded Lf-Nps was assessed by MTT assay. Briefly, 5 × 10³ Rb Y79 total and sorted cells were suspended in 90 µL complete RPMI-1640 medium and seeded into 96-well plates for overnight incubation. The cells were treated with a series of concentrations of standard CPT, ETP, Lf-CPT, and Lf-ETP (5–300 µM equivalents) and incubated for 48 hours. After incubation, 20 µL of 5 mg/mL MTT reagent was added to each well and incubated for 3 hours. The Formazan crystals formed were dissolved in 100 µL dimethyl sulfoxide (DMSO), and the absorbance was measured at 595 nm using a multiplex plate reader (TECAN, Mannedorf, Switzerland). Cell viability was calculated and compared with the controls for each of the population, and half-maximum inhibitory concentrations (IC₅₀) were calculated using the GraphPad Prism version 6 software (GraphPad Software, La Jolla, CA, USA).

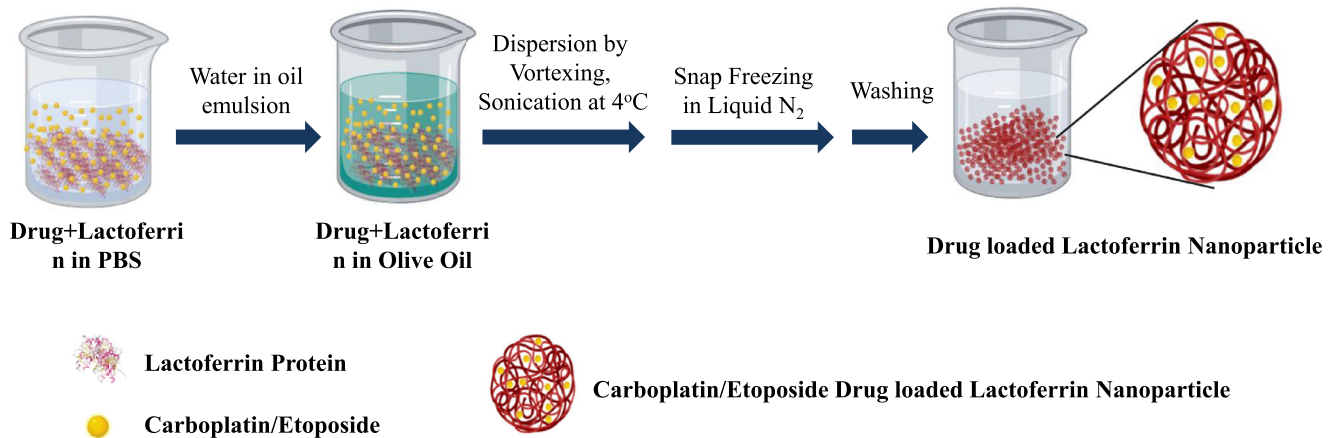


FIGURE 1. Diagrammatic representation of CPT- or ETP-loaded Lf-Nps synthesis using solution-oil-based chemistry.

Statistical Analysis

The quantitative data were stated as mean (SD), and GraphPad Prism version 6 (GraphPad Software) was used for two-way ANOVA with Sidak’s multiple comparison test used for drug uptake and free drug available in conditioned media and two-way ANOVA with Tukey’s multiple comparison test for cytotoxicity of all experimental groups. The experiments were repeated at least three times with biological replicates. $P < 0.05$ was considered for statistically significant differences between the groups.

RESULTS

Preparation and Characterization of Drug-Loaded Lf-Nps

The schematic of drug-loaded Lf-Nps preparation is described in Figure 1. The Lf-Nps were homogeneous and spherical in shape, and the mean (SD) size was 14.13 (1.08) nm, as seen in the transmission electron microscope (TEM). The size of the particle increased up to a mean (SD) of 61.2 (3.94) nm and 45.15 (5.85) nm after loading CPT and ETP, respectively (Figs. 2a–c).

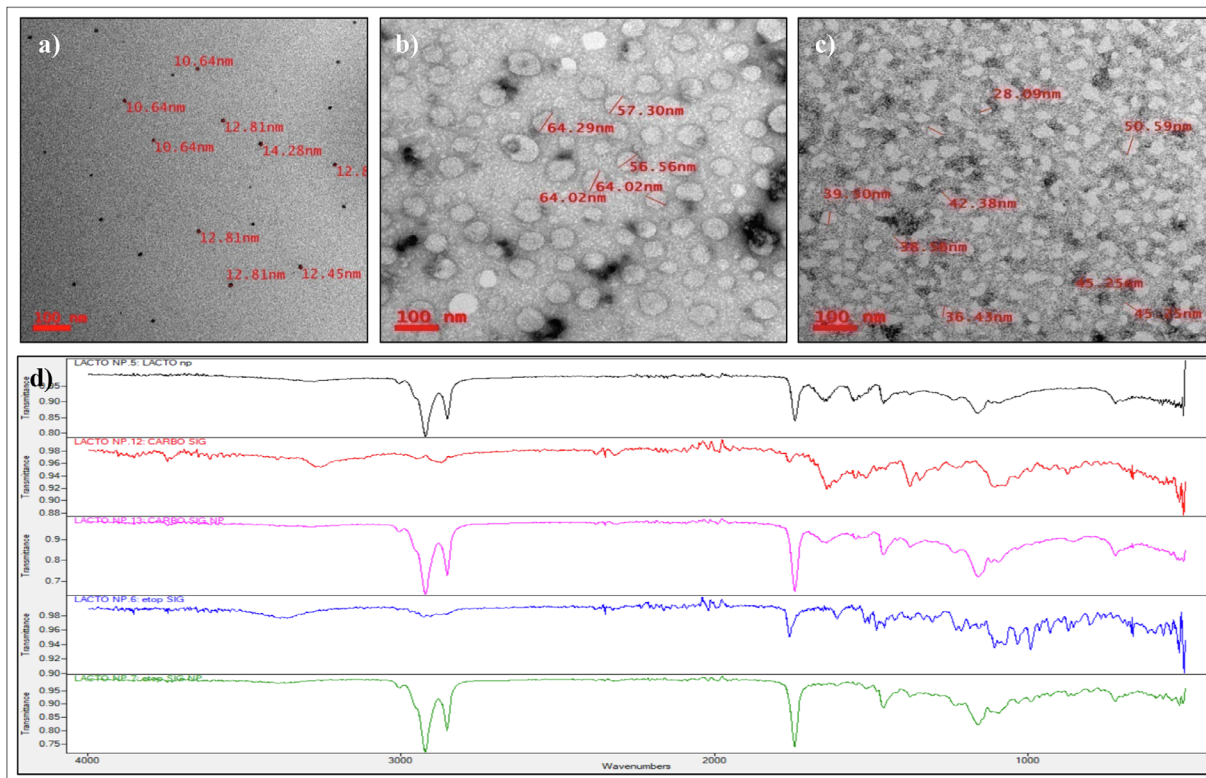


FIGURE 2. Physicochemical characterization of CPT- or ETP-loaded Lf-Nps. Transmission electron microscopy images of (a) Lf-Nps, (b) Lf-CPT, and (c) Lf-ETP and (d) FTIR spectrum analysis of Lf-CPT and Lf-ETP (blank nanoparticle, black; CPT, red; Lf-CPT, pink; ETP, blue; Lf-ETP, green).

TABLE 1. Variation Band Frequencies Exhibited by Functional Groups in CPT and Lf-CPT

Functional Groups	Band Frequencies in CPT (cm ⁻¹)	Band Frequencies in Lf-CPT (cm ⁻¹)
N-H	3270	3280
C-H stretch	2949, 2870	2922, 2852
C=O	1760, 1692	1744, 1691
N-H bend	1632	1632
C-H bend	1461, 1377	1462, 1377
C-O	1287, 1228	1277, 1235

TABLE 2. Variation Band Frequencies Exhibited by Functional Groups in ETP and Lf-ETP

Functional Groups	Band Frequencies in ETP (cm ⁻¹)	Band Frequencies in Lf-ETP (cm ⁻¹)
C-H stretch	2927, 2855	2923, 2853
C=O	1761	1745
C=C (aromatic)	1609	1609
C-H bend	1457, 1375	1458, 1376
C-O (Acyl)	1305, 1229	1305, 1230
C-O (alkoxy)	1157, 1093, 1033	1159, 1094, 1032

The ATR-FTIR analysis of nanoformulated drugs revealed the characteristic bands of functional groups with a slight shift in the nanoformulated drugs when compared to the pure drugs (Fig. 2d). The band frequencies of the functional groups are listed in Tables 1 and 2. No major variation in

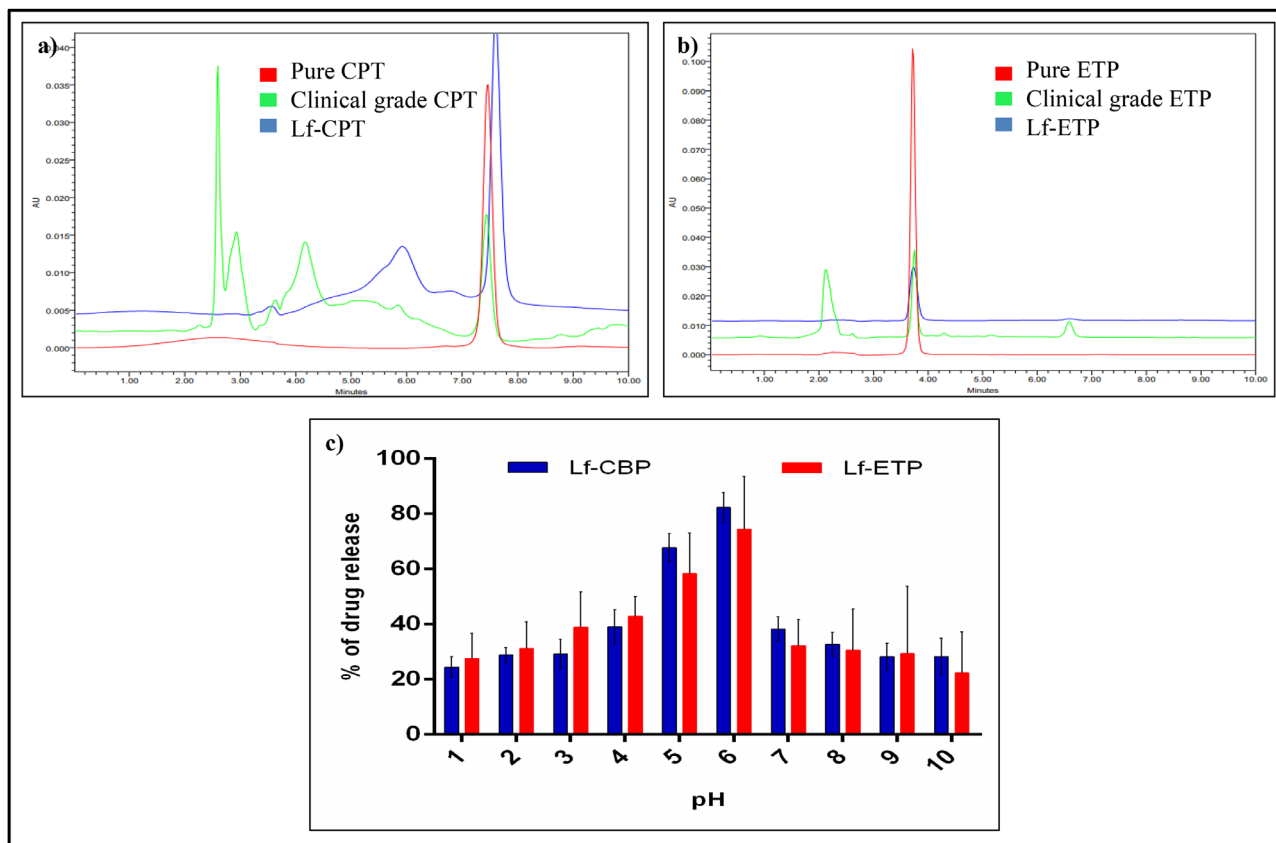
the bond frequencies was observed between pure drug and nanoparticle except for C=O bond and C-H stretch. The C=O bond was 1760, 1761 cm⁻¹ for pure drug and 1744, 1745 cm⁻¹ for nanoformulations, and the C-H stretch was 2949, 2870 cm⁻¹ for pure CPT and 2922, 2852 cm⁻¹ for Lf-CPT. The slight shift in the stitching frequency indicates that the drug in the Lf-Nps is stabilized by noncovalent interaction without significant variation in the structure of the drugs. Blank Lf protein nanoparticles also showed similar bands at 1745 cm⁻¹ and 2921, 2852 cm⁻¹.

Evaluation of Loading Efficiency and pH-Dependent Drug Release of Lf-Nps Loaded With CPT and ETP. Mean (SD) encapsulation efficiency of Lf-CPT and Lf-ETP was 59.63% (8.02%) and 38.05% (4.75%), respectively. The mean (SD) loading capacity for CPT and ETP was 11.92% (1.6%) and 7.61% (0.95%), respectively (Supplementary Information 1–4). The retention time analyzed by HPLC separation showed that pure CPT, clinical-grade CPT, and CPT released from Lf-CPT had a retention time of 7.5 minutes (Fig. 3a). Similarly, pure ETP, clinical-grade ETP, and ETP released from Lf-ETP had a retention time of 3.7 minutes (Fig. 3b).

The peak drug release from Lf-CPT (82.3 µg/mL) and Lf-ETP (74.4 µg/mL) was observed at pH 6 (Fig. 3c).

Isolation and Characterization of Cancer Stem Cells in Rb Y79 Cells

As evaluated by fluorescence-activated cell sorting (FACS), CD133^{lo} cells constituted a mean (SD) of 15% (0.32%) cells (Figs. 4a, 4b). They were sorted using MACS with a purity

**FIGURE 3.** Physicochemical characterization of CPT- or ETP-loaded Lf-Nps. HPLC analysis of standard drugs and Lf-Nps (a) CPT and (b) ETP (c) pH-dependent drug release of Lf-CPT and Lf-ETP.

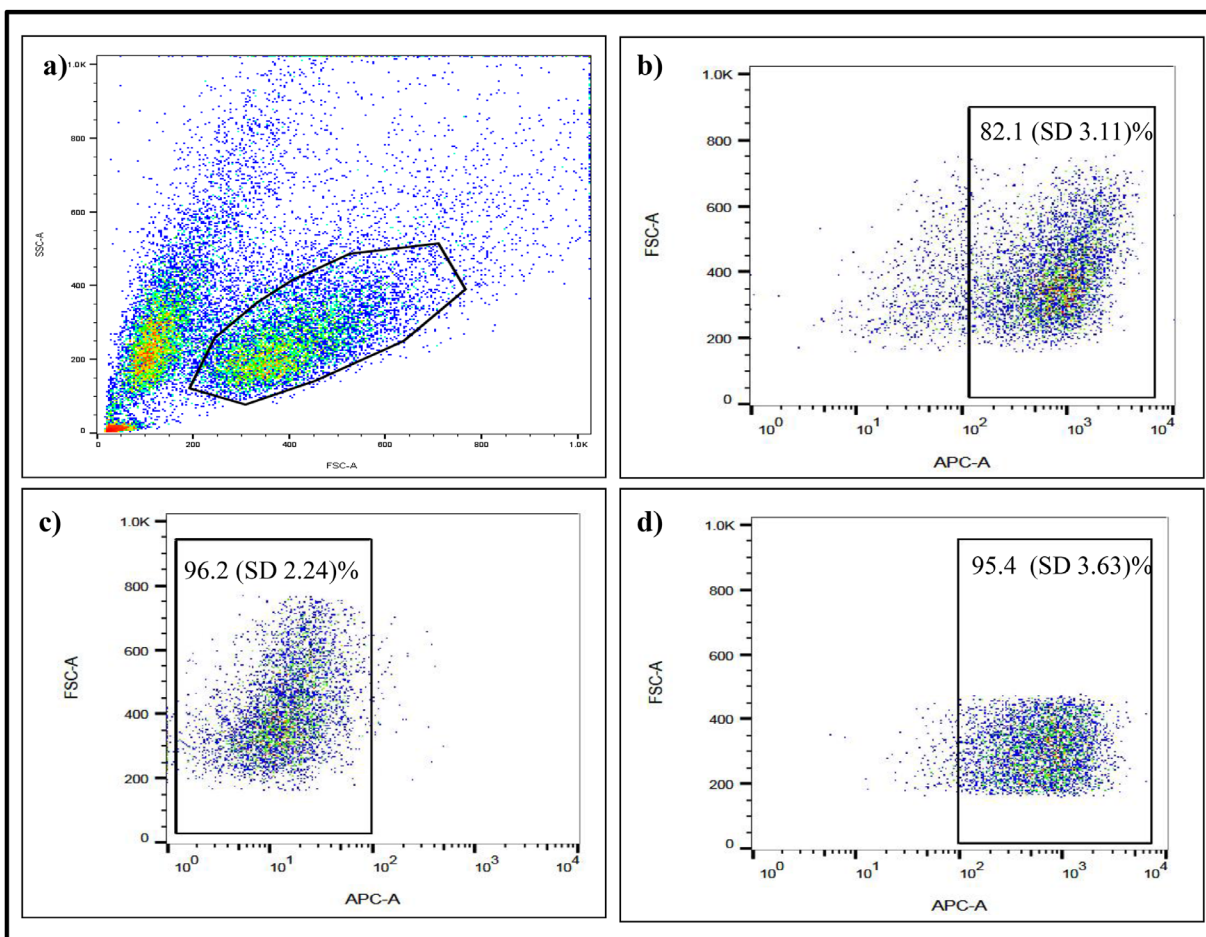


FIGURE 4. Flow cytometry analysis of CD133 expression in Rb Y79 cell line. (a) Scatterplot of Y79 cells with gating around the live population, (b) CD133-APC expression, and MACS sorting purity of (c) CD133^{lo} population and (d) CD133^{hi} population of Rb Y79 cells.

of $\geq 90\%$ and with a cell viability of $\geq 95\%$ after sorting (Figs. 4c, 4d).

Quantitative Measurement of Drug Uptake of Rb Y79 Cells. The cellular uptake of standard CPT and ETP resulted in higher uptake at 30 minutes and then reduced over 4 hours. However, the uptake of Lf-CPT and Lf-ETP increased over time from 30 minutes to 4 hours in a linear manner followed by a stepwise reduction until 48 hours ($P < 0.0001$) (Fig. 5a).

Cellular Uptake of Lf-Nps by Confocal Microscopy

Based on confocal microscopy analysis, we noted that the free R6G was absorbed quickly by the Rb Y79 cells in 30 minutes, followed by slow and complete elimination by 4 hours. In contrast, the Lf-R6G accumulated slowly in Rb Y79 cells and was retained up to 8 hours (Fig. 5b).

Quantitative Measurement of Drug Uptake by Rb Y79 CSCs and Non-CSCs. As seen with a UV-Vis spectrophotometer, the cellular uptake of CPT, ETP, Lf-CPT, and Lf-ETP was significant in both Rb Y79 CSCs and non-CSCs. However, the cellular uptake of Lf-CPT and Lf-ETP was increased when compared to their soluble counterparts ($P < 0.0001$), irrespective of cell types (Figs. 6a, 6c). The cellular uptake of soluble and drug-loaded Lf-Nps is shown

in Table 3, and multiple-comparison P values of CPT versus ETP and Lf-CPT versus Lf-ETP are shown in Table 4.

Estimation of Free Drug in Conditioned Media of Rb Y79 CSCs and Non-CSCs. The concentration of CPT and ETP in the conditioned media of RbY79 CSCs and non-CSCs treated with CPT, ETP, Lf-CPT, and Lf-ETP was linear. However, the concentration of CPT and ETP was higher in the conditioned media of cells treated with standard drugs when compared to the drug-loaded Lf-Nps of both Rb Y79 CSC and non-CSC conditioned media ($P < 0.0001$). Similarly, the free drug concentration was significantly higher in the conditioned media of Rb Y79 CSCs compared to the non-CSCs ($P < 0.0001$), treated with standard and drug-loaded Lf-Nps over a 48-hour duration (Figs. 6b, 6d). The free drug concentration of standard and drug-loaded Lf-Nps-treated Rb Y79 CSCs and non-CSCs is shown in Table 3.

Cytotoxic Effect of Lf-Nps and Standard and Drug-Loaded Lf-Nps on Y79 Rb CSCs and Non-CSCs. The cytotoxic effect of Lf-Nps and Standard and Drug-Loaded Lf-Nps on Y79 Rb CSCs and non-CSCs was evaluated after 48 hours of drug treatment. The Lf-Nps did not reveal any cytotoxic effect on both Rb CSCs and non-CSCs even at higher concentrations (Fig. 7a), and the in vitro cytotoxicity analysis showed that the cytotoxic effect of Lf-CPT and Lf-ETP was higher in total Rb Y79 cells compared to the standard CPT ($P < 0.0001$) and ETP ($P < 0.0001$),

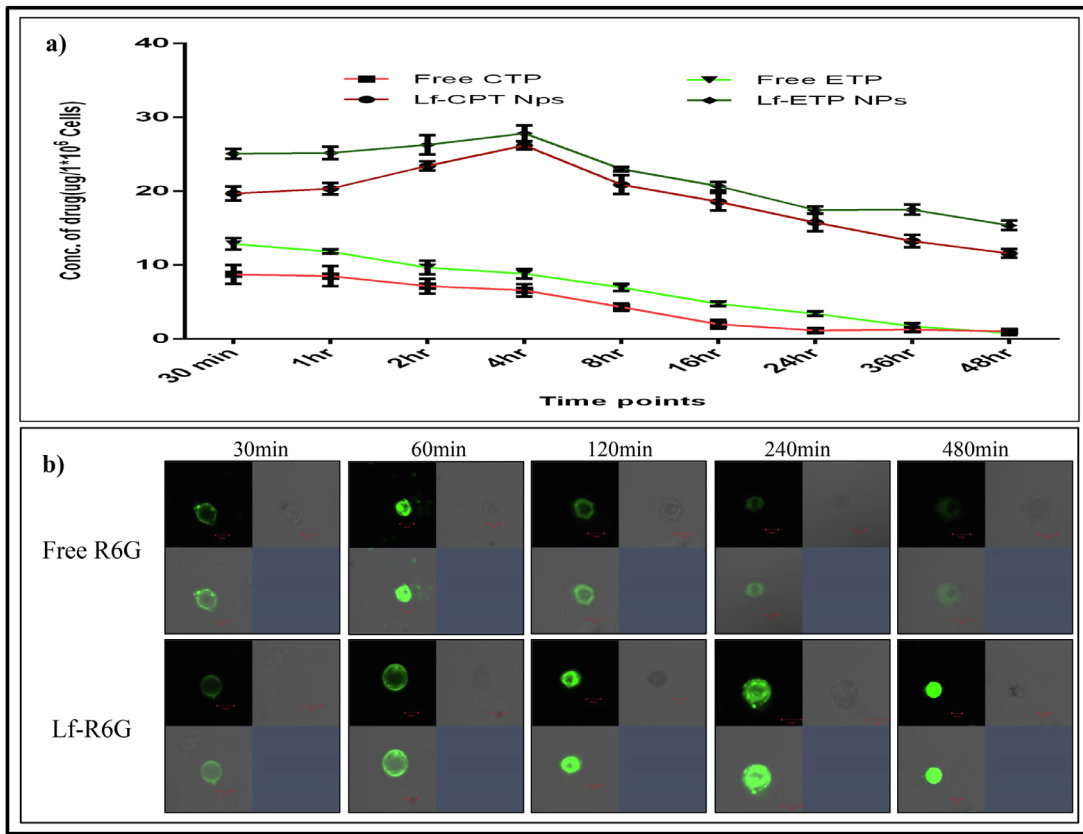


FIGURE 5. Quantitative measurement of drug uptake. (a) Quantitative measurement of cellular drug uptake of standard drug and drug-loaded Lf-Nps. (b) Cellular uptake of soluble R6G and Lf-R6G in Rb Y79 cells at different time points.

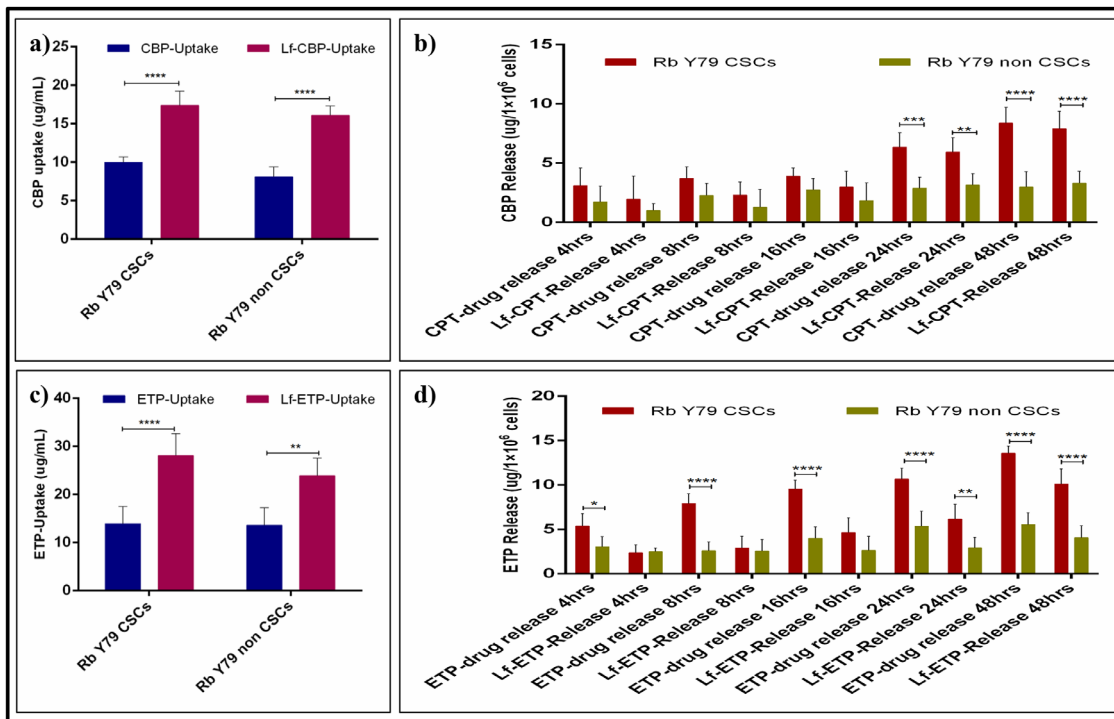


FIGURE 6. Quantitative measurement of drug uptake and release in Rb Y79 CSCs and non-CSCs. (a) Standard CPT and Lf-CPT drug uptake Rb Y79 CSCs and non-CSCs. (b) CPT available in conditioned media after drug treatment of CSCs and non-CSCs at different time points. (c) Standard ETP and Lf-ETP drug uptake Rb Y79 CSCs and non-CSCs and (d) ETP available in conditioned media after drug treatment of CSCs and non-CSCs at different time points (* $P < 0.05$, ** $P < 0.01$, *** $P < 0.001$, and **** $P < 0.0001$).

TABLE 3. Quantitative Uptake and Drug Concentration Available in Conditioned Media of Free CPT, Lf-CPT, Free ETP, and Lf-ETP on Rb Y79 CSCs and Non-CSCs

Characteristic	Drug Uptake ($\mu\text{g}/10^6$ Cells), Mean (SD)	Drug Concentration in CM After 48 Hours ($\mu\text{g}/10^6$ Cells), Mean (SD)	Drug Retention (%) Into the Cells After 48 Hours
Free CPT-Rb Y79 CSCs	9.99 (0.7)	8.37 (1.34)	15.46
Lf-CPT-Rb Y79 CSCs	17.38 (1.84)	7.92 (1.47)	54.43
Free CPT-Rb Y79 non-CSCs	8.09 (1.29)	2.97 (1.32)	63.28
Lf-CPT-Rb Y79 non-CSCs	16.1 (1.2)	3.31 (1.01)	79.44
Free ETP-Rb Y79 CSCs	13.9 (3.57)	13.59 (0.77)	2.23
Lf-ETP-Rb Y79 CSCs	28.07 (4.56)	10.11 (1.7)	63.98
Free ETP-Rb Y79 non-CSCs	13.61 (3.64)	5.55 (1.33)	59.40
Lf-ETP-Rb Y79 non-CSCs	23.87 (3.67)	4.07 (1.35)	82.94

TABLE 4. P Values of Two-Way ANOVA With Sidak's Multiple Comparison for Drug Uptake

Data	Multiple Comparison	P Value
CBP vs. ETP	Y79 CSCs/CBP vs. Y79 CSCs/ETP	0.1853
	Y79 CSCs/CBP vs. Y79 non-CSCs/CBP	0.8542
	Y79 CSCs/CBP vs. Y79 non-CSCs/ETP	0.2510
	Y79 CSCs/ETP vs. Y79 non-CSCs/CBP	0.0155
	Y79 CSCs/ETP vs. Y79 non-CSCs/ETP	>0.9999
Lf-CBP vs. Lf-ETP	Y79 non-CSCs/CBP vs. Y79 non-CSCs/ETP	0.0219
	Y79 CSCs/Lf-CBP vs. Y79 CSCs/Lf-ETP	0.0003
	Y79 CSCs/Lf-CBP vs. Y79 non-CSCs/Lf-CBP	0.9889
	Y79 CSCs/Lf-CBP vs. Y79 non-CSCs/Lf-ETP	0.0221
	Y79 CSCs/Lf-ETP vs. Y79 non-CSCs/Lf-CBP	0.0001
	Y79 CSCs/Lf-ETP vs. Y79 non-CSCs/Lf-ETP	0.2625
	Y79 non-CSCs/Lf-CBP vs. Y79 non-CSCs/Lf-ETP	0.0062

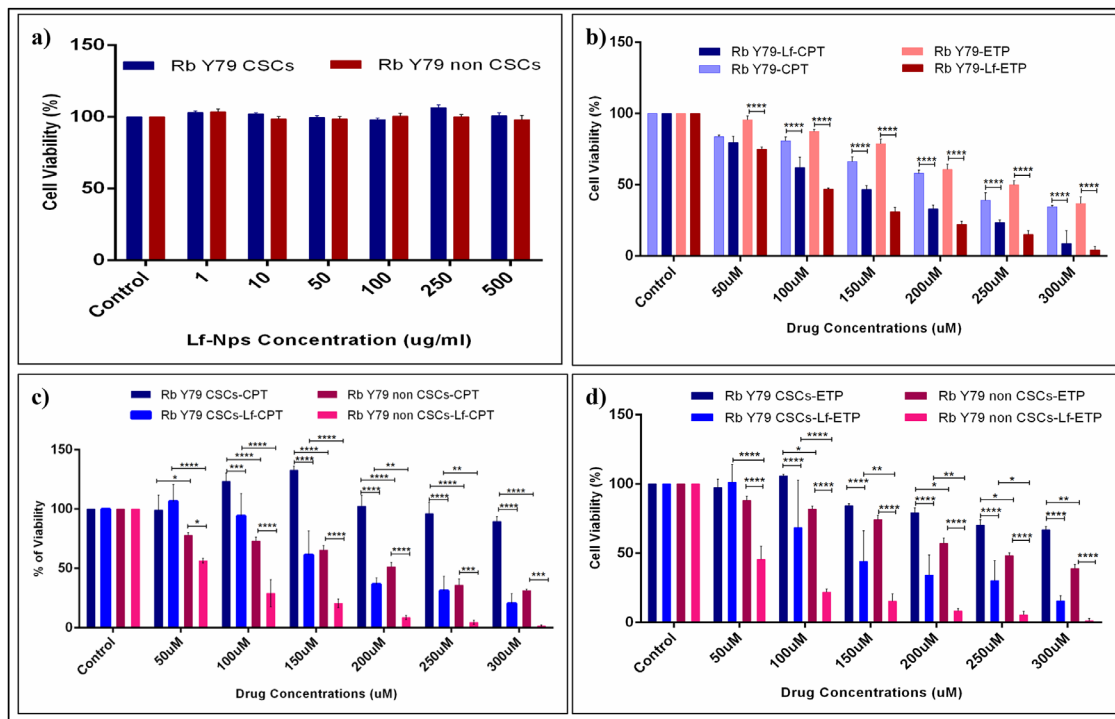


FIGURE 7. Cytotoxicity of Lf-Nps, standard drug and drug-loaded Lf-Nps on total Rb Y79 cells, CSCs (CD133^{lo}), and non-CSCs (CD133^{hi}). (a) Cytotoxicity of Lf-Nps on Rb Y79 CSCs and Rb Y79 non-CSCs. (b) Cytotoxicity of standard CPT, ETP, Lf-CPT, and Lf-ETP on total Rb Y79 cells. (c) Cytotoxicity of standard CPT versus Lf-CPT on Rb Y79 CSCs and non-CSCs. (d) Cytotoxicity of standard ETP versus Lf-ETP on Rb Y79 CSCs and non-CSCs (*P < 0.05, **P < 0.01, ***P < 0.001, ****P < 0.0001).

TABLE 5. IC₅₀ Values of Free CPT, Lf-CPT, Free ETP, and Lf-ETP on Total Rb Y79 CSCs and Non-CSCs

Characteristic	Rb Y79 Total Cells	Rb Y79 CSCs	Rb Y79 Non-CSCs
Free CPT	110.4	230.3	144.4
Lf-CPT	89.48	118.2	59.41
Free ETP	143.7	198.1	173.5
Lf-ETP	71.5	129	43.27

respectively (Fig. 7b). Similar to total Rb Y79 cells, the cytotoxic effect of CPT and ETP was higher in Rb Y79 non-CSCs cells compared to the Rb Y79 CSCs ($P < 0.0001$), whereas Lf-CPT and Lf-ETP cytotoxic effect increased in both Rb Y79 CSCs and non-CSCs compared to the standard CPT ($P < 0.0001$) and ETP ($P < 0.0001$) (Figs. 7c, 7d). The IC₅₀ values of CPT, ETP, Lf-CPT, and Lf-ETP of total Rb Y79, CSCs, and non-CSCs are shown in Table 5.

DISCUSSION

One of the key characteristic features of CSCs is drug resistance, and this feature is believed to be responsible for the tumor recurrence after drug treatment.²⁵ Therapeutic targeting of CSCs in early disease makes an effective treatment strategy for cancer cure. Tumor recurrence in Rb is not uncommon after chemotherapy²⁶ and could be due to multiple factors, including the presence of CSCs, drug resistance, as well as reactivation of retinocytoma-like areas within the tumor.^{13,27} Our earlier study documented the presence of drug resistance in the CSC population of Rb cell lines,¹⁶ so in this study, we focused on overcoming the drug resistance of CSCs through nanoformulated drugs. Our study shows that the Lf-Nps loaded with CPT and ETP clearly demonstrated increased drug uptake, retention, and cytotoxicity of Lf-CPT and Lf-ETP compared to standard drugs, more so in the CSC population.

In our study, Lf was used as a drug carrier of clinical-grade CPT and ETP. Lf is an iron-transporting glycoprotein belonging to the transferrin family. Receptors of Lf are highly expressed in tumor cells because of the enhanced iron demand of rapidly dividing metabolically active tumor cells,²⁸ including Rb Y79 cells.²⁹ Drug-loaded Lf-Nps were prepared by oil-solution method,²⁴ in contrast to other protein nanoparticles,³⁰ and therefore it is a cost-effective, simple, and fast procedure without chemical modification of native Lf protein. The nanoparticles were uniformly distributed, spherical in shape, and smaller than previously reported Lf-CPT (68–81 nm),²⁴ which could possibly be due to the preparation of Lf-Nps with clinical-grade CPT. The Lf-ETP nanoparticles were synthesized by the same method, and size was noted to be smaller than other nanoparticles such as poly(lactic-co-glycolic acid) (PLGA) and polycaprolactone (PCL).³¹ The FTIR analysis confirmed that CPT and ETP were stable in Lf-Nps, but the functional group bands were slightly shifted, and there was some variation in the bond frequencies as previously reported for Lf-CPT by our group.²⁴ The encapsulation efficiency of Lf-CPT was higher than previously reported (52%), while the Lf-ETP was lower compared to the Lf-CPT, ETP-loaded PLGA, and PCL.³¹ Higher encapsulation efficiency and loading capacity of CPT compared with ETP could be due to the structural differences between CPT and ETP. The pH-dependent drug release assay showed that Lf-CPT and Lf-ETP release was

higher at pH 6, which concurs with our previous results of Lf-Nps prepared with carmustine, zidovudine, efavirenz, and lamivudine.^{32,33} It also substantiates the predicted property of Lf-Nps to release maximum drugs in slightly acidic conditions, which is an advantageous feature of nanoparticles to reduce systemic toxicity and target tumor cells only. Cellular uptake studies showed that Lf-CPT and Lf-ETP enter the cells within 30 minutes and remains intracellular for a longer time compared to their standard forms, which again concurs with our previous study involving Lf-Nps prepared by CPT, oxaliplatin, and 5-fluorouracil.^{24,34} Although not exclusively evaluated in this study, the longer retention time of Lf-CPT and Lf-ETP possibly indicates receptor-mediated endocytosis,²⁴ while the standard drugs diffuse passively and are effluxed by the drug resistance proteins.³⁵ The prolonged drug retention, irrespective of the mechanism, is the most favorable factor in clinical settings, as it enhances cytotoxicity and also activates apoptotic pathways.

In this current study, the intracellular drug uptake of Lf-Nps was explored by loading the R6G fluorescence dye and compared with free R6G. The soluble R6G passively diffused into the cells and was eliminated rapidly over 4 hours, whereas the Lf-R6G entered into the cells and was retained for a longer time, similar to the previously reported Lf-Nps loaded with CPT, zidovudine, efavirenz, and lamivudine.^{24,33}

Similar to other solid tumors,³⁶ Rb also harbors CSCs,¹³ which we identified as CD133⁺ cells in the Rb Y79 cell line.¹⁶ CD133 (prominin) is a well-characterized biomarker to identify and isolate CSCs. CD133⁺ cells exhibit CSC properties in many tumors: gliomas, glioblastomas, and breast and ovarian cancers.³⁷ In contrast to this evidence, CD133⁻ cells are known to form the tumor mass in animal models of glioblastoma^{37,38} and ovarian cancer³⁹; these cells are resistant to therapeutic drugs in Rb.¹⁶ The hallmark feature of CSCs is resistance to chemotherapeutic drugs due to the presence of drug efflux proteins, DNA damage response, or cells in a quiescent state.²⁵ A significant increase in drug uptake was observed in Lf-CPT and Lf-ETP compared to soluble CPT and ETP over a 4-hour incubation in both Rb CSCs and non-CSCs. After 4 hours of drug uptake, the concentration of free CPT and ETP in the conditioned media of both CSCs and non-CSCs was higher in standard CPT- and ETP-treated cells as compared to the nanoformulated drugs, more so in Rb Y79 CSCs. This may be due to the uptake, adsorption, or internalization of the drug-loaded Lf-Nps. Although we did not pursue the mechanism in this study, we speculate that they may be released at a desirable environment (possibly pH 6) through the active drug exporter proteins. This observation is supported by Zhao et al.,⁴⁰ who reported that the drug release from Mesenchymal Stem Cells (MSCs) is higher in free doxorubicin (DOX) compared to the PLGA-DOX nanoparticles. The release of standard drugs and drug-loaded Lf-Nps was significantly higher in Rb CSCs than non-CSCs. This may be due to high expression of the drug exporter proteins (i.e., ABCG2, ABCB5, MDR1) in Rb CSCs. ABCG2 has been identified by multiple studies in Rb and is known to be highly expressed in CSCs, contributing to drug resistance.^{16,41} Despite the decreased release of drug-loaded Lf-Nps from Rb Y79 cells, the most promising finding in this study is that the in vitro cytotoxic effect of nanoformulations was significantly increased compared to the standard drugs, specifically in the Rb Y79 CSC population. The increased cytotoxicity of the drug-loaded Lf-Nps clearly suggests that drug resistance of CSCs can be overcome, which is the most desired effect from a clinical point of view.

The present study is novel and highlights the notable efficacy of drugs loaded on Lf-Nps as compared to the standard counterparts. However, our study does have some weaknesses. The foremost limitation of this study is that, due to lack of expression of CD44 in Rb Y79 cells, we had to depend on a negative marker (CD133⁻) for CSC enrichment, unlike other tumors and primary Rb with a couple of CSC markers (CD44⁺/CD133⁻). Although the cell viability was good with MACS sorting, the purity of CD133-enriched and CD133-depleted populations was over 95%, which possibly can be enhanced using FACS. Second, the drug available in conditioned media was estimated from the free drug concentration of treated cells, but the protein-bound drug and the drug present on the surface of the cells and wedges were not estimated. Further validation studies to estimate the total drug concentration and the drug-releasing mechanism would improve our understanding of the drug release mechanism. It would also be worthwhile to evaluate the efficacy of different drug combinations loaded with Lf-Nps along with in vivo testing in Rb CSC xenograft models, in order to pave the way for clinical application.

CONCLUSION

This in vitro study documents the increased efficacy of CPT- and ETP-loaded Lf-Nps with significantly increased cellular uptake, sustained intracellular drug retention, and increased cytotoxicity up to ~50%, more specifically in the CSC population in Rb Y79 cells. This is a very promising step that could be further validated in primary Rb and in vivo Rb tumor models, in order to explore its clinical potential to target CSCs in Rb and other ocular malignancies.

Acknowledgments

The authors thank the UGC-UKIERI, DST Nano mission, UPE-II, and DST PURSE-II, University of Hyderabad for supporting this project. NRVL is grateful to the Council of Scientific & Industrial Research (CSIR, India) for awarding Junior Research Fellowship. PJ is grateful to the Department of Biotechnology (DBT, India) for awarding Junior Research Fellowship. RMN is grateful to University Grant Commission (UGC, India) for awarding Senior Research Fellowship. VP and RM are grateful to UGC-UKIERI for project fellowship. The authors also acknowledge the flow cytometry and confocal facilities at the University of Hyderabad.

Supported by UGC-UKIERI, academic research grants from the DST-PURSE (University of Hyderabad), and UPE-II (University of Hyderabad). NRVL is supported by CSIR, Government of India (Junior Research Fellowship (JRF)); PJ is supported by DBT, India (JRF); and RMN is supported by UGC, India (Senior Research Fellowship (SRF)). The funding body had no role in the design of the study and collection, analysis, and interpretation of data and in writing the manuscript.

Disclosure: **R.V.L. Narayana**, None; **P. Jana**, None; **N. Tomar**, None; **V. Prabhu**, None; **R.M. Nair**, None; **R. Manukonda**, None; **S. Kaliki**, None; **S.E. Coupland**, None; **J. Alexander**, None; **H. Kalirai**, None; **A.K. Kondapi**, None; **G.K. Vemuganti**, None

References

- Dimaras H, Kimani K, Dimba EA, et al. Retinoblastoma. *Lancet*. 2012;379(9824):1436–1446.
- Honavar S, Reddy V, Ali M. Distant metastatic retinoblastoma without central nervous system involvement. *Indian J Ophthalmol*. 2013;61(7):357.
- Khosravi A, Shahrabi S, Shahjehani M, Saki N. The bone marrow metastasis niche in retinoblastoma. *Cell Oncol*. 2015;38(4):253–263.
- Bakhshi S, Meel R, Radhakrishnan V. Current therapy and recent advances in the management of retinoblastoma. *Indian J Med Paediatr Oncol*. 2012;33(2):80.
- Kaliki S, Retinoblastoma Shields C.: achieving new standards with methods of chemotherapy. *Indian J Ophthalmol*. 2015;63(2):103.
- Shields CL, Lally SE, Leahey AM, et al. Targeted retinoblastoma management: when to use intravenous, intra-arterial, periocular, and intravitreal chemotherapy. *Curr Opin Ophthalmol*. 2014;25(5):374–385.
- Chévez-Barrios P, Eagle RC, Krailo M, et al. Study of unilateral retinoblastoma with and without histopathologic high-risk features and the role of adjuvant chemotherapy: a Children's Oncology Group study. *J Clin Oncol*. 2019;37(31):2883–2891.
- Yanık Ö, Gündüz K, Yavuz K, Taçyıldız N, Ünal E. Chemotherapy in retinoblastoma: current approaches. *Türk Oftalmol Derg*. 2015;45(6):259–267.
- Ali MJ, Gupta R, Vemuganti GK, Honavar SG. Histopathology of retinoblastoma after primary chemotherapy. In: *Proceedings of the XIV International Congress of Ocular Oncology*. Cambridge, UK: 2009:296.
- Chen J, Li Y, Yu T-S, et al. A restricted cell population propagates glioblastoma growth after chemotherapy. *Nature*. 2012;488(7412):522–526.
- Zhao J. Cancer stem cells and chemoresistance: the smartest survives the raid. *Pharmacol Ther*. 2016;160:145–158.
- Hermann PC, Bhaskar S, Cioffi M, Heeschen C. Cancer stem cells in solid tumors. *Semin Cancer Biol*. 2010;20(2):77–84.
- Seigel GM, Campbell LM, Narayan M, Gonzalez-Fernandez F. Cancer stem cell characteristics in retinoblastoma. *Mol Vis*. 2005;11:729–737.
- Hu H, Deng F, Liu Y, et al. Characterization and retinal neuron differentiation of WERI-Rb1 cancer stem cells. *Mol Vis*. 2012;18:2388–2397.
- Balla MMS, Vemuganti GK, Kannabiran C, Honavar SG, Murthy R. Phenotypic characterization of retinoblastoma for the presence of putative cancer stem-like cell markers by flow cytometry. *Invest Ophthalmol Vis Sci*. 2009;50(4):1506.
- Nair RM, Balla MMS, Khan I, Kalathur RKR, Kondaiah P, Vemuganti GK. In vitro characterization of CD133lo cancer stem cells in Retinoblastoma Y79 cell line. *BMC Cancer*. 2017;17(1):779.
- Valent P, Bonnet D, De Maria R, et al. Cancer stem cell definitions and terminology: the devil is in the details. *Nat Rev Cancer*. 2012;12(11):767–775.
- Zeuner A. The secret life of quiescent cancer stem cells. *Mol Cell Oncol*. 2015;2(1):e968067.
- Abdullah LN, Chow EK. Mechanisms of chemoresistance in cancer stem cells. *Clin Transl Med*. 2013;2:3.
- Qin W, Huang G, Chen Z, Zhang Y. Nanomaterials in targeting cancer stem cells for cancer therapy. *Front Pharmacol*. 2017;8:1.
- Jain A, Singh SK, Arya SK, Kundu SC, Kapoor S. Protein nanoparticles: promising platforms for drug delivery applications. *ACS Biomater Sci Eng*. 2018;4(12):3939–3961.
- Parveen S, Sahoo SK. Evaluation of cytotoxicity and mechanism of apoptosis of doxorubicin using folate-decorated chitosan nanoparticles for targeted delivery to retinoblastoma. *Cancer Nanotechnol*. 2010;1(1–6):47–62.

23. Das M, Sahoo SK. Folate decorated dual drug loaded nanoparticle: role of curcumin in enhancing therapeutic potential of nutlin-3a by reversing multidrug resistance. *PLoS ONE*. 2012;7(3):e32920.
24. Ahmed F, Ali MJ, Kondapi AK. Carboplatin loaded protein nanoparticles exhibit improve anti-proliferative activity in retinoblastoma cells. *Int J Biol Macromol*. 2014;70:572–582.
25. Dean M, Fojo T, Bates S. Tumour stem cells and drug resistance. *Nat Rev Cancer*. 2005;5(4):275–284.
26. Shields CL. Development of new retinoblastomas after 6 cycles of chemoreduction for retinoblastoma in 162 eyes of 106 consecutive patients. *Arch Ophthalmol*. 2003;121(11):1571.
27. Chung J, Turaka K, Shields CL. Retinocytoma shows lack of response to chemoreduction. *J Pediatr Ophthalmol Strabismus*. 2010;47(6):e1–e3.
28. Kanwar JR, Samarasinghe RM, Sehgal R. Nano-lactoferrin in diagnostic, imaging and targeted delivery for cancer and infectious diseases. *J Cancer Sci Ther*. 2012;4(3):031–042.
29. Samuel J, Singh N, Kanwar JR, Krishnakumar S, Kanwar RK. Upregulation of sodium iodide symporter (NIS) protein expression by an innate immunity component: promising potential for targeting radiosensitive retinoblastoma. *Exp Eye Res*. 2015;139:108–114.
30. Govender T. PLGA nanoparticles prepared by nanoprecipitation: drug loading and release studies of a water soluble drug. *J Controlled Release*. 1999;57(2):171–185.
31. Snehalatha M, Venugopal K, Saha RN. Etoposide-loaded PLGA and PCL nanoparticles I: preparation and effect of formulation variables. *Drug Deliv*. 2008;15(5):267–275.
32. Athmakur H, Kondapi AK. Carmustine loaded lactoferrin nanoparticles demonstrates an enhanced antiproliferative activity against glioblastoma in vitro. *Int J Appl Pharm*. 2018;10(6):234.
33. Kumar P, Lakshmi YS, Kondapi AK. Triple drug combination of zidovudine, efavirenz and lamivudine loaded lactoferrin nanoparticles: an effective nano first-line regimen for HIV therapy. *Pharm Res*. 2017;34(2):257–268.
34. Ahmed F, Kumari S, Kondapi AK. Evaluation of antiproliferative activity, safety and biodistribution of oxaliplatin and 5-fluorouracil loaded lactoferrin nanoparticles for the management of colon adenocarcinoma: an in vitro and an in vivo study. *Pharm Res*. 2018;35(9):178.
35. Ritter CA, Jedlitschky G, Meyer zu Schwabedissen H, Grube M, Köck K, Kroemer HK. Cellular export of drugs and signaling molecules by the ATP-binding cassette transporters MRP4 (ABCC4) and MRP5 (ABCC5). *Drug Metab Rev*. 2005;37(1):253–278.
36. Visvader JE, Lindeman GJ. Cancer stem cells in solid tumours: accumulating evidence and unresolved questions. *Nat Rev Cancer*. 2008;8(10):755–768.
37. Barzegar Behrooz A, Syahir A, Ahmad S. CD133: beyond a cancer stem cell biomarker. *J Drug Target*. 2019;27(3):257–269.
38. Beier CP, Beier D. CD133 negative cancer stem cells in glioblastoma. *Front Biosci Elite Ed*. 2011;3:701–710.
39. Kusumbe AP, Mali AM, Bapat SA. CD133-expressing stem cells associated with ovarian metastases establish an endothelial hierarchy and contribute to tumor vasculature. *Stem Cells*. 2009;27(3):498–508.
40. Zhao Y, Tang S, Guo J, et al. Targeted delivery of doxorubicin by nano-loaded mesenchymal stem cells for lung melanoma metastases therapy. *Sci Rep*. 2017;7(1):44758.
41. Shukla A, Srivastava A, Kumar S, et al. Expression of multidrug resistance proteins in retinoblastoma. *Int J Ophthalmol*. 2017;10(11):1655–1661.